AD_____

Award Number: W81XWH-04-1-0916

TITLE: Molecular Imaging with Quantum Dots Probing EMT and Prostate Cancer Metastasis in Live Animals

PRINCIPLE INVESTIGATOR: Leland W. K. Chung, Ph.D.

CONTRACTING ORGANIZATION: Emory University
Atlanta, GA 30322

REPORT DATE: October 2005

TYPE OF REPORT: Annual

PREPARED FOR: U.S. Army Medical Research and Materiel Command
Fort Detrick, Maryland 21702-5012

REPORT DOCUMENTATION PAGE

Form Approved
OMB No. 0704-0188

1. REPORT DATE	2. REPORT TYPE	3. DATES COVERED
01-10-2005	Annual	1 Oct 2004 – 30 Sep 2005

4. TITLE AND SUBTITLE

Molecular Imaging with Quantum Dots Probing EMT and Prostate Cancer Metastasis in Live Animals

5a. CONTRACT NUMBER

5b. GRANT NUMBER
W81XWH-04-1-0916

5c. PROGRAM ELEMENT NUMBER

6. AUTHOR(S)

Leland W. K. Chung, Ph.D.

5d. PROJECT NUMBER

5e. TASK NUMBER

5f. WORK UNIT NUMBER

7. PERFORMING ORGANIZATION NAME(S) AND ADDRESS(ES)

Emory University
Atlanta, GA 30322

8. PERFORMING ORGANIZATION REPORT NUMBER

9. SPONSORING / MONITORING AGENCY NAME(S) AND ADDRESS(ES)
U.S. Army Medical Research and Materiel Command
Fort Detrick, Maryland 21702-5012

10. SPONSOR/MONITOR'S ACRONYM(S)

11. SPONSOR/MONITOR'S REPORT NUMBER(S)

12. DISTRIBUTION / AVAILABILITY STATEMENT
Approved for Public Release; Distribution Unlimited

13. SUPPLEMENTARY NOTES
Original contains colored plates: ALL DTIC reproductions will be in black and white.

14. ABSTRACT

SEE ATTACHED PAGE

15. SUBJECT TERMS
Quantum dots

16. SECURITY CLASSIFICATION OF:				18. NUMBER OF PAGES	19a. NAME OF RESPONSIBLE PERSON
					USAMRMC
a. REPORT	b. ABSTRACT	c. THIS PAGE			19b. TELEPHONE NUMBER *(include area code)*
U	U	U	UU	25	

Standard Form 298 (Rev. 8-98)
Prescribed by ANSI Std. Z39.18

Abstract

Despite the development of various animal and tissue culture models for the study of human prostate cancer growth and metastasis, there is no non-invasive model that provides real-time information on the behavior of prostate cancer cells in the prostate or at distant sites. The goal of this application is to devise a highly sensitive and specific nanotechnology- based molecular imaging technique to detect prostate cancer growth locally and at distant sites and observe the interaction between prostate cancer cells and their local microenvironment during their acquisition of migratory, invasive and metastatic capabilities. This technique was made possible by a close collaboration between Chung/Zhau, who have extensive experience in the development of human prostate cancer metastatic models, and Nie, a biomedical engineer who devised an ultrasensitive and specific nanotechnology quantum dot (QD) bioconjugate that can image cancer cells in live animals at a sensitivity close to the single cell level. This collaborative interaction between Chung/Zhau/Nie could significantly improve our ability to diagnose, prognose and treat human prostate cancer, first in experimental models and later in the clinic. We have proposed three highly interactive aims that allow the PIs and trainees to interact during the development of this highly innovative technology. Aim 1 is to synthesize and test QD conjugates for the molecular imaging of prostate cancer cells in culture, and to improve the quality of the QDs so they will emit light at the near-infrared range for potential detection of cancer cells located in deep tissues. Aim 2 is to develop a highly reproducible and metastatic human prostate cancer model using immunocompromised mice. Aim 3 is to combine Aim 1 and 2 by testing the sensitivity and the specificity of the molecular probe in detecting prostate cancer metastasis and its interaction with tumor microenvironment through the important process of epithelial-to-mesenchymal transition (EMT), which has been closely associated with cancer cell migration and invasion, and appears at the invasion front of many cancers. Upon completion of this proposed interactive project, we hope to further improve this technology to visualize cancer in live animals and perform real-time studies of the molecular interaction between cancer and its microenvironment.

Table of Contents

Introduction:

Androgen independence and bone metastasis are two lethal phenotypes of human prostate cancer. The current project has three proposed aims. They are: 1) To develop a highly sensitive quantum dot (QD) bioconjugate imaging methodology for the detection of prostate cancer cells in live animals; 2) To develop a highly sensitive and reproducible human prostate cancer bone and visceral metastasis model for studying the molecular steps associated with human prostate cancer progression; and 3) To probe tumor-stroma interaction with special emphasis on interrogating the biological basis of the epithelial-to-mesenchymal transition (EMT) *in vivo* using QD nanotechnology for molecular imaging. In this funding period, we have achieved the following goals:

Body:

Task 1: Develop and characterize nanoparticle QD antibody conjugates capable of binding to prostate cancer cell surface specific antigens (months 1 to 12).

We have evaluated five different EMT related markers using quantum dot (QD) multiplexing technology. These markers are: E-cadherin, N-cadherin, vimentin, receptor activator of NFκB ligand (RANKL), and IL13 receptor α2. Some of these markers (E-cadherin, N-cadherin, and IL13 receptor α2) are cell surface receptors, others are intracellular proteins (vimentin and RANKL). These molecular markers are currently explored as biomarkers indicative of EMT.

We have recently submitted a manuscript, which has now been accepted for publication in *The Prostate* with an online publication date of August 10, 2006 (see attached, Appendix 1).

Task 2: Evaluate the sensitivity and specificity of the nanoparticle QD antibody conjugates for molecular imaging of human prostate cancer cells and their variants with defined differences in biochemical and behavioral characteristics (months 6 to 12).

We have developed and characterized an ARCaP model of EMT using the above described molecular markers as indication of this transition. A manuscript is currently in draft, which describes the assessment of these molecular biomarkers using immunohistochemistry, RT-PCR, and Western blot.

As described in Task 1, the manuscript by Xu et al. entitled "Prostate cancer metastasis: Role of the host microenvironment in promoting epithelial to mesenchymal transition and increased bone and adrenal gland metastasis" has been published online on August 10, 2006 in *The Prostate* (Appendix 1).

Task 3: Test the ability of selected molecular imaging probes to be used together (multiplexing) for tracking single or aggregated cells in culture (months 6 to 12).

We have successfully developed the multiplexing technologies as described under Task 1 to evaluate EMT in a human ARCaP EMT model. We have compared the expression of these molecular markers in cultured cells and in tumor specimens harvested from mice inoculated with ARCaP cells.

Figures 1 to 5 showed the concept of EMT in prostate carcinogenesis (Figure 1). We have determined a series of genes associated with prostate EMT using ARCaP model. Figures 3 to 5 showed the multiplexing of EMT-associated genes using quantum dot conjugated antibody as probes for the detection of EMT biomarkers in both human prostate cancer cells (Figures 3 and 4) and tissues (Figure 5).

Task 4: Select quantum dot molecular probes with far-red and near-infrared emitting wave lengths for *in vivo* imaging in animals previously implanted with human prostate tumors (months 12 to 36).

We have developed far red and near infrared probe for the detection of cell surface PSMA protein in LNCaP model of human prostate cancer progression. This same technique will be applied for the detection of E-cadherin and IL13 receptor α 2 expression in ARCaP EMT model.

We have completed PSMA-QD 800nm for the visualization of human prostate tumors in mouse bone (see Shi et al. AACR abstract, 2006, Appendix 2).

Task 5: Develop and characterize an ARCaP human prostate cancer cell model with a predictable pattern of bone and soft tissue metastases (months 1 to 24).

We have established the concept upon interaction between ARCaP cells and mouse bone; it promotes EMT in ARCaP model of human prostate cancer progression. The resultant ARCaP cells with mesenchymal phenotype was shown to gain increased bone and adrenal gland metastases (See Appendix 1).

Task 6: Do molecular profiling of ARCaP and ARCaP-derivative cell lines with respect to their gene expression using cDNA microarray and validate such differences using tissue array (months 6 to 18).

We are currently developing technologies using LNCaP model of human prostate cancer progression as a model to validate gene expression profiles, validated by immunohistochemistry of human tissues and cell lines. This technology combined with tissue array will be applied to ARCaP model and expanded to human prostate cancer specimens.

Task 7: Assess gene expression profiles in tumors obtained from animals that have been subjected to imaging and characterize gene expression profiling in primary and metastatic tumors using RT-PCR, Western blots and IHC (months 18 to 36).

To be completed.

Task 8: Develop a nanotechnology-based prostate cancer detection technology for both local invasion and distant metastasis with particular focus on EMT in primary and distant metastatic sites (months 1 to 24).

We have completed in part this task. We are currently exploring the use of this technology for the validation of EMT in both primary and metastatic ARCaP tumors in live mice (See Appendix 1 and 2).

Task 9: Evaluate the sensitivity and specificity of individual nanoparticle QD antibody conjugates as molecular probes for multiplexing numerous cell surface targets simultaneously in mice previously implanted with human ARCaP cells or derivative variants (months 12 to 36).

In progress.

Task 10: Summarize the results, repeat certain studies, and prepare manuscripts for publication (months 12 to 36).

We have submitted one abstract for publication summarizing our progress in probe development, multiplexing technology, and application to animal and human tissue specimens (See Appendix 2 and Figures 3-5).

Key Research Accomplishments:

- We have developed an ARCaP model of human prostate cancer progression with focus on EMT.
- We have developed far red and infrared range of quantum dot nanoparticles for *in vivo* imaging of prostate cancer cells in live mice.
- We have developed multiplexing technology to evaluate EMT biomarkers during ARCaP prostate cancer progression.

Reportable Outcomes:

1. We are currently in preparation of two manuscripts dealing with the use of quantum dot nanotechnology in the detection of EMT in ARCaP model of human prostate cancer progression.
2. We submitted an abstract for AUA to study EMT in human renal cancers.

Conclusions:

Quantum dot linked molecules have been shown to be highly effective in the detection of molecular biomarkers associated with EMT in the ARCaP model of human prostatic cancer progression. This technology can be expanded to determine EMT in clinical human prostate cancer tissues.

References:

None

Appendix:

1. Xu J, Wang R, Xie ZH, Odero-Marah V, Pathak S, Multani A, Chung LWK, Zhau HE. (2006). Prostate cancer metastasis: Role of the host microenvironment in promoting epithelial to mesenchymal transition and increased bone and adrenal gland metastasis. *The Prostate*, Epub August 10, 2006.
2. Shi C, Xie ZH, Hsieh C-L, Nie S, Zhau HE, and Chung LWK, (2006). An ultrasensitive imaging technique utilizing near-infrared fluorescent quantum dots for the detection of human prostate cancer bone metastasis in a mouse xenograft model. Abstract. 2006 AACR Annual Conference.
3. Nomura T, Huang W-C, Xing Y, Young AN, Marshall FF, Nie S, Zhau HE, and Chung LWK. Cell signaling mediated by b2-microglobulin and protein kinase A promotes growth and epithelial to mesenchymal transition in human renal cancers. Abstract. 2006 AUA meeting.

Prostate Cancer Metastasis: Role of the Host Microenvironment in Promoting Epithelial to Mesenchymal Transition and Increased Bone and Adrenal Gland Metastasis

Jianchun Xu,[1] Ruoxiang Wang,[1] Zhi Hui Xie,[1] Valerie Odero-Marah,[1] Sen Pathak,[2] Asha Multani,[2] Leland W.K. Chung,[1] and Haiyen E. Zhau[1]*

[1]*Department of Urology, Molecular Urology and Therapeutics Program, Emory University School of Medicine, Atlanta, Georgia*
[2]*Department of Cancer Biology and Laboratory Medicine, the University of Texas M. D. Anderson Cancer Center, Houston, Texas*

BACKGROUND. The ARCaP cell line was established from the ascites fluid of a patient with metastatic prostate cancer. This study characterized the host microenvironmental role in cancer progression, epithelial to mesenchymal transition (EMT), and bone and adrenal metastasis in parental ARCaP and its derived cell subclones.
METHODS. Cytogenetic profiles, growth, migration, invasion, cellular interaction, drug sensitivities, and gene expression of ARCaP cell subclones were compared. In vivo gene expression, behavior, and metastasis of ARCaP subclones were analyzed by serial intracardiac injections into SCID mice.
RESULTS. $ARCaP_E$ cells, with cobblestone morphology, underwent EMT through cellular interaction with host bone and adrenal gland. Lineage-derived $ARCaP_M$ cells, with spindle-shape fibroblastic morphology, exhibited decreased cell adhesion and increased metastasis to bone and adrenal gland. Cytogenetic analyses of parental and ARCaP subclones confirmed their clonality.
CONCLUSIONS. ARCaP uniquely models the molecular basis of prostate cancer bone and adrenal metastases and epithelial to mesenchymal transition.

KEY WORDS: **organ-specific tropism; clonal interaction; cancer cell heterogeneity; animal model; cancer progression**

INTRODUCTION

The diversity and heterogeneity of human prostate cancer cells is well appreciated. A broad spectrum of cancer cell behaviors include the ability to grow, invade surrounding normal tissues, and metastasize to distant organs [1–3]. Despite similarities in the histologic presentation of prostate cancers at the time of disease diagnosis, their clinical behaviors, including time to disease progression and metastasis, sensitivity to hormones, chemotherapy and radiation, and propensity to relapse still cannot be predicted with certainty [4–7]. Relevant models that could probe the phenotype, behavior, and progression of cancer cells are lacking, as well as appropriate methods and sensitive biomarkers that can diagnose disease and reliably predict its

Abbreviations: ARCaP, androgen refractory cancer of the prostate; EMT, epithelial mesenchymal transition.

*Correspondence to: Haiyen E. Zhau, PhD, Department of Urology, Molecular Urology and Therapeutics Program, Emory University School of Medicine, 1365B Clifton Rd. NE, Atlanta, GA 30322.
E-mail: hzhau@emory.edu
Received 17 February 2006; Accepted 16 May 2006
DOI 10.1002/pros.20488
Published online in Wiley InterScience (www.interscience.wiley.com).

clinical behavior early on. However, investigations have revealed a wealth of fresh information on the molecular basis of cancer metastasis through: (1) the development of useful transgenic [8–10] and xenograft [11–18] animal models and human prostate cancer cell lines [3]; (2) characterization of the genetic diversity and heterogeneity of cancer cells and animal models; (3) the identification of specific loci that may harbor genes or clusters of genes contributing to the development of familial or sporadic forms of prostate cancer [19–21]; and (4) elucidation of intracellular cell signaling and the roles of autocrine and paracrine factors in the tumor milieu that control the behavior of prostate cancer cells in interaction with the tumor microenvironment [2,3,22–24]. Because prostate cancer has a predilection to metastasize to bone, resulting in increased patient mortality and morbidity, we sought to develop a highly metastatic prostate cancer model to evaluate the involvement of epithelial to mesenchymal transition (EMT) and the host microenvironment in prostate cancer bone and soft tissue metastases. This communication reports the cytogenetic, phenotypic, and behavioral characterizations and gene expression profiles of parental ARCaP and ARCaP cell subclones subsequent to cellular interaction with mouse host cells in vivo.

MATERIALS AND METHODS

Cell Culture

ARCaP cells were derived by our laboratory from the ascites fluid of a patient with metastatic carcinoma of the prostate [16]. Cells were routinely maintained in a culture medium consisting of T medium (Life Technologies, Gaithersburg, MD) and 5% fetal bovine serum (FBS) at 37°C supplemented with 5% CO_2. Limited dilution was performed by suspending 400 cells in 60 ml of T medium and seeding 100 μl per well in six 96-well plates. The wells containing one cell were expanded. Cell growth was determined by crystal violet assay [25]. In brief, cells (3×10^4 per well) were trypsinized and resuspended in T medium and seeded in 24-well plates under routine culture conditions. One plate of cells was removed at each designated time point and fixed with 0.5 ml of 1% glutaraldehyde for 15 min, stained with 0.5% crystal violet solution for 15 min, rinsed four times with water, air dried then eluted by Sorenson's solution for 30 min at room temperature. The optical density of the eluted solutions was read at 590 nm. The OD_{590} was determined by an APECTRAmax 190 Microplate Reader and directly correlated with the number of cells [25]. Conditioned media (CM) were collected from cells reaching 80% confluence, rinsed with PBS, replaced with serum-free T media and 2% TCM (Celox Laboratories, Inc., St. Paul, MN) and cultured for 24 hr. The effects of CM on cell growth were determined in triplicate assays of three independent experiments with data expressed as average ± SEM.

Invasion and Migration Assays

A total of 35 μl of Matrigel Matrix (BD Biosciences, Bedford, MA; 100 $\mu g/cm^2$ surface area; diluted 1:5 in T medium) was placed on the inner upper Boyden chamber (BIOCOAT, 6.4 mm insert with 8 μm pores; Becton Dickinson Labware, Bedford, MA) and incubated for 30 min prior to adding to the cells. Cells (5×10^4) were suspended in 500 μl of 0.1% BSA/T medium and added to the inner upper Boyden chamber. One milliliter of 0.1% BSA/T medium was added to the outer Boyden chamber. The chambers with or without Matrigel were placed in 24-well plates and incubated for 48 hr. MTT solution (2.5 mg/ml; Sigma, St. Louis, MO) was added to both the inner (40 μl) and the outer (80 μl) chambers and incubated for an additional 4 hr. The media were collected separately from each chamber, and cell-associated MTT crystals were scrubbed off with filter paper and dissolved separately in 500 μl dimethyl sulfuroxide (DMSO). The color intensity was measured at 590 nm against the appropriate blank controls (0.1% BSA/T medium with MTT solution and 500 μl DMSO). The % invasion was calculated by MTT eluted from cells invaded through the Boyden chamber/MTT eluted from cells that remained in the upper Boyden chamber plus those that invaded through the Boyden chamber. The % migration was conducted and calculated similarly to cell invasion, except the Boyden chambers were not coated with Matrigel [26,27]. Relative invasion, migration, and growth are presented as average ± SEM of triplicate assays from two independent experiments.

In addition, migration was also determined by scratch wound assay [28] where cells (5×10^5) were cultured in a 24-well plate. Then the 100% confluent cell layers were wounded with two parallel scratches using a sterile 200 μl pipette tip and rinsed with PBS. Images were taken at 0, 12, 24, 36, and 48 hr at the marked site using a ZEISS Axiovert 200 M inverse light microscope (at 4×) and Openlab software (Improvision, Coventry, UK). Five measurements were taken from 0 to 48 hr. Mean widths were determined as a function of time with % migration tabulated as (Width 0 hr − Width at 12 to 48-hr) ÷ Width 0 hr × 100%.

Chemotherapeutic Sensitivity of Parental ARCaP and ARCaP Cell Subclones

Cells (5×10^3 per well) were cultured in 96-well plates for 24 hr and then replaced with fresh cultured

medium to which were added Paclitaxel, Etoposide, or Doxorubicin (Sigma, St. Louis, MO) at four different concentrations, followed by incubation for 96 hr. Cell growth was measured using the MTT assay.

Cytogenetic Analysis

Cells at 75% confluence in fresh media were exposed to Colcemid (20 ng/ml; Sigma) for 30 min at 37°C, rinsed two times with Hanks' balanced salt solution, and exposed to 0.01% trypsin for 5–7 min. The dislodged cells were neutralized with RPMI 1640 containing 10% FBS, and centrifuged at 1,700 rpm for 5 min. The cell pellet was disturbed and exposed to a hypotonic solution (0.06 M KCl) for 20 min at room temperature. After centrifugation, the cells were fixed in acetic acid: methanol (1:3, v/v) for 15 min, rinsed three times with the fixative and stained with Giemsa solution for G-banding following routine procedures [16]. Five to ten G-banded metaphase spreads were photographed for chromosome analyses for each cell clone.

Protein Expression

Immunohistochemical (IHC) and Western blot were used to determine the level of protein expression in cells. Monoclonal antibodies against cytokeratin 18/19 (CK18/19) were obtained from Santa Cruz Biotechnology, Inc. (Santa Cruz, CA); vimentin (VM) antibody from Dako Corp., Ltd. (Carpinteria, CA). Polyclonal antibodies to E-cadherin and N-cadherin were obtained from Santa Cruz. For immunohistochemical analysis, acetone (−20°C)-fixed cells or deparaffinized tissue sections (4 μ) were treated with 3% hydrogen peroxide, blocked with Super Block (Scytek Laboratories, Logan, UT), avidin and biotin (Vector Laboratories, Inc., Burlingame, CA) for 15 min each, and incubated with primary antibody overnight at 4°C. The signals were amplified by an avidin–biotin HRP system using multilink and label reagents (BioGenex, San Ramon, CA) and hydrogen peroxide/DAB (3, 3′-diaminobenzidine) as peroxidase substrate and chromogen (Sigma). Background activity was determined by (1) eliminating the primary antibody, (2) using matching mouse immunoglobulin subtypes, or (3) normal goat or rabbit serum at appropriate dilutions. For Western Blot Analysis, cells were harvested at 80% confluence and rinsed twice with cold PBS. Cellular protein was extracted in a homogenization buffer (phosphate buffered saline with 1% Nonidet P-40, 0.5% sodium deoxycholate, 0.1% SDS, 10 mg/ml phenylmethylsulfonyl fluoride (PMSF), 1 mM sodium orthovanadate, 1 μg/ml leupeptin, and 1 μg/ml aprotinin). The total cell lysate (7.5–20 μg) was resolved by 7.5 or 10–20% SDS–polyacrylamide gel electrophoresis and transferred to a nitrocellulose membrane (NitroPure, Osmonics, Westborough, MA). The membrane was blocked for 1 hr at room temperature with 5% nonfat milk in TBST buffer (50 mM Tris-HCl, 150 mM NaCl, 0.05% Tween 20) and incubated with primary antibody in TBST blocking buffer for 1 hr at room temperature. The signal was detected by reacting with secondary antibody conjugated to horseradish peroxidase coupled with enhanced chemiluminescence (ECL) reagents (Amersham-Pharmacia Biotech, Piscataway, NJ), and exposed on Hyperfilm (Amersham).

Tumorigenicity and Metastasis In Vivo

Five to seven-week-old athymic NCr-nu/nu male mice (NCI) were used as hosts. Cells at 80% confluence were changed with fresh T-medium the day before harvest. Cells were resuspended (2×10^7/ml) and injected subcutaneously (1×10^6 cells/100 μl/site, four sites per mouse). For intracardiac injection, cells were injected as 5×10^5 cells/50 μl PBS/mouse using a 28G1/2 needle. Mice were anesthetized and placed in a supine position. The needle was inserted 5 mm above the middle of the left side of sternum. When fresh arterial blood appeared in the syringe, this indicated the successful penetration into the left ventricle. Cells were infused slowly and directly into mouse left ventricle for systemic circulation. Tumor formation was monitored weekly and volume calculated as length × width × height × 0.5236 [25,26]. Metastases to distant organs were confirmed by radiography, necropsy, and histomorphology of the tumor specimens.

Derivation of Cell Subclones From Tumor Tissues

Tumor tissue was freshly harvested, rinsed three times with PBS, replaced with cold PBS with antibiotics (Penicillin/Streptomycin (10,000 U/ml), placed on ice for 5 min, changed to cold T medium with 10% FBS and antibiotics, and kept on ice. Tissue was cut into 0.5–1 mm^3 pieces, put in cell culture dishes (separating at 0.5–1.0 cm), and briefly air dried to allow attachment. One to 2 drops of culture media were added on top of and around the tissue pieces to keep them humid and incubated. A few more drops of media were added 6 hr later followed by more media at 24 and 48 hr. Tumor cells and mouse stromal cells started to emerge by 48 hr with spindle-shape cells around the tissue and epithelial-like cells migrating away from the tissue piece, forming a rather ''pure'' colony by Day 7–10. We used cloning disks (Scienceware, Pequannock, NJ) to isolate pure cell subclones. Additional contaminating stromal cells were removed from epithelial cells by differential trypsinization [26].

RESULTS

ARCaP Subclones Have Similar Cytogenetic Profiles but Distinct Morphology, Growth Rates, Gene Expression Profiles and Behaviors In Vitro

The ARCaP cells were originated from the ascites fluid of a patient with prostate cancer bony metastasis [16]. The ARCaP cells harbor wild type androgen receptor (AR) and secrete low level of prostatic specific antigen (PSA) as compared to LNCaP cells. In contrast to LNCaP cells, parental ARCaP cells are invasive and cell growth is repressed by androgen both in vitro and in vivo. Figure 1 shows five ARCaP cell subclones obtained by dilution cloning with marked differences in their morphology, ranging from cobblestone epithelial (IF11 or $ARCaP_E$) to spindle-shape mesenchymal cells (IA8 or $ARCaP_M$). Clones IID4 and IIC11 gave rise to morphologic features intermediate between $ARCaP_E$ and $ARCaP_M$. One of the subclones, IF3, exhibited giant cell morphology with multinuclear features resembling matured osteoclasts. The growth rates of the five ARCaP cell subclones in vitro showed the mesenchyme-like $ARCaP_M$ as the fastest, followed by IIC11, IID4, and IF3, with the epithelium-like $ARCaP_E$ being the slowest (data not included).

Cytogenetic Analyses

Cytogenetic analyses of parental ARCaP and the five cell subclones (Table I) indicated that these cells are clonal. These subclones exhibited the same major marker chromosomes as ARCaP parental cells [16]. However, each of the ARCaP cell subclones had its unique marker chromosomes. During the course of this study, both the morphology and the cytogenetic profiles of parental ARCaP and its subclones were stable despite repeated subculturing of the respective cells in vitro for more than 20 passages (unpublished results). The ARCaP cytogenetic profile [16] is distinct from the widely studied LNCaP cells [26]. They do not share common marker chromosomes and can easily be identified and distinguished from each other based on their distinctive marker chromosomes. While the ARCaP subclones have distinct cytogenetic profiles, they also differ in their histomorphology, growth rate, migratory, invasive, and metastatic potentials, and drug sensitivity (see Results). These properties are maintained in the mixed parental ARCaP cells by cell–cell interaction.

Growth, Migration, and Invasion of $ARCaP_E$ and $ARCaP_M$ Subclones In Vitro

Since EMT has been associated with increased cancer cell invasion and migration [29–31], we evaluated the possible correlation between two morphologically distinct ARCaP subclones, cobblestone-shaped $ARCaP_E$ and the spindle-shaped $ARCaP_M$ subclones. Cell invasion using a Boyden Chamber coated with a Matrigel barrier (Fig. 2A), and migration as assessed by Scratch Wound Assay (Fig. 2B) correlated with cell growth rates (Fig. 2C), revealed higher migration and invasion by $ARCaP_M$ than $ARCaP_E$ cells ($P < 0.01$). These two clones, after co-culturing (1:1) for more than 20 passages, still retained their original distinct morphology as seen in Figure 1 without one clone being preferentially ''selected'' over the other (data not included). We hypothesize that clonal interaction

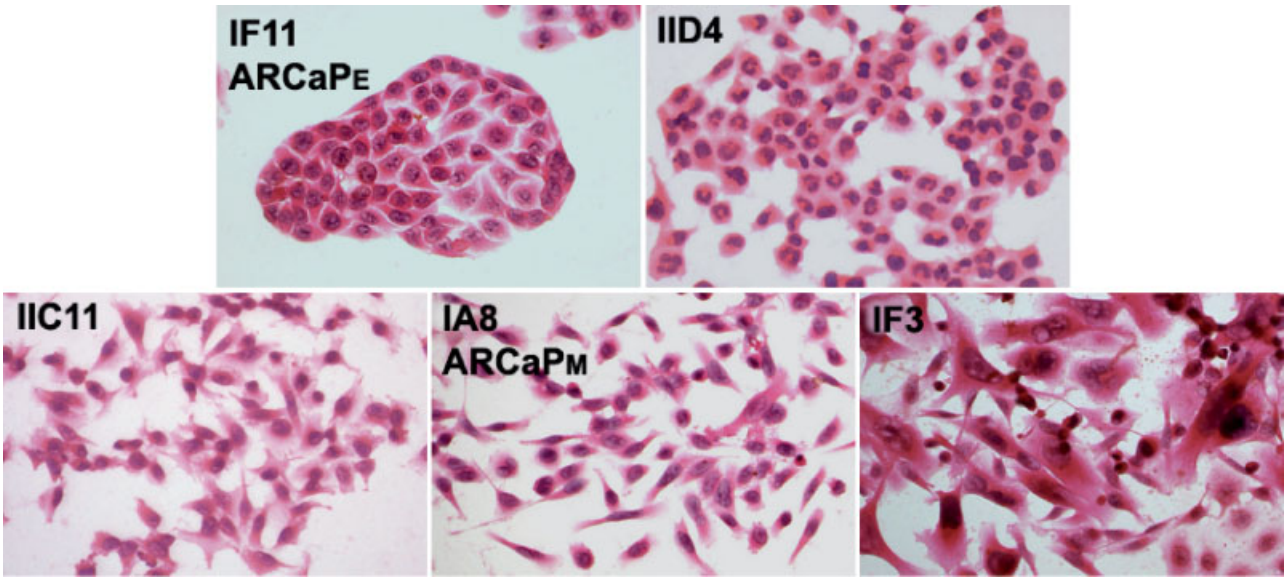

Fig. 1. Histomorphology of ARCaP cell subclones ranged from cobblestone-shaped $ARCaP_E$ to spindle-shaped $ARCaP_M$ cells.

TABLE I. Cytogenetic Profiles of Parental ARCaP and Its Five Cell Subclones

Cells	1p+	1q+	del5q	5p+	6p+	del8p	i(9q)	12q+	15p+	18q+	21p+	delX	t(13:15)	8q+	i(5q)	6q+
IIC11	+	+	+	+	+	+	+	+	+	+	+	+	−	−	−	−
ARCaPM	+	+	+	+	+	+	+	+	+[a]	+	+	+	+[b,a]	−[a]	−	−
ARCaPE	+	+	+	+	+	+	+	+	−[a]	+	+	+	−[a]	+[b,a]	−	−
IID4	+	+	+	+	+	−	+	+	+	+	+	+	−	−	+[b]	−
IF3	+	−	+	+	+	+	+	+	+	+	+	+	−	−	−	+[b]
ARCaP	+	−	+	+	+	+	−	+	−	+	−	+	−	−	−	−

[a]Difference between $ARCaP_M$ and $ARCaP_E$.
[b]Difference among the five subclones.

occurs through factors secreted by one cell type exerting either a growth stimulatory or inhibitory effect on the other. To test this hypothesis, we replaced the cultured media of $ARCaP_E$ with conditioned media (CM) collected from $ARCaP_M$ and vice versa. Figure 3 showed that CM from the fast-growing $ARCaP_M$ cells stimulated the growth of the slow-growing $ARCaP_E$ cells ($P < 0.01$), but there was no growth inhibitory effect when the reverse experiment was conducted. These results suggest that a stimulatory rather than inhibitory factor plays a role in the maintenance of $ARCaP_E$ and $ARCaP_M$ subclones within the ARCaP cell population (see below).

Gene Expression Profiles of ARCaP Subclones Grown in Culture

We conducted gene profile analysis of ARCaP subclones with specific emphasis on $ARCaP_E$, $ARCaP_M$, and ARCaP-Ad (Adrenal). We found that, consistent with their morphologic features, $ARCaP_E$ expressed dominantly epithelial markers while $ARCaP_M$ and ARCaP-Ad expressed mesenchymal markers (Fig. 4), as evaluated by Western blots and IHC. These results were also confirmed by RT-PCR (data not included). Because of these morphologic and molecular characteristics thus the names $ARCaP_E$, $ARCaP_M$, and $ARCaP_{Ad}$ were given to IF11, IA8, and ARCaP-Adrenal subclones respectively. $ARCaP_E$ expressed higher E-cadherin and cytokeratins 18 and 19 typically associated with epithelial cells, whereas $ARCaP_M$ and $ARCaP_{Ad}$ expressed more genes associated with mesenchymal cells, such as elevated vimentin and N-cadherin expression with concomitantly lower expression of epithelium-associated E-cadherin and cytokeratin genes. In addition to the classic EMT-associated genes, we also detected elevated protein expression of PSA, AR, and PSMA and two new EMT-associated genes in $ARCaP_M$ than that in $ARCaP_E$ (data not included).

Effects of Chemotherapeutic Agents on In Vitro Growth of ARCaP Cell Subclones

Because ARCaP represents a lethal form of human prostate cancer with the ability to invade and metastasize aggressively to bone and soft tissues, we sought to determine the in vitro sensitivities of $ARCaP_E$ and

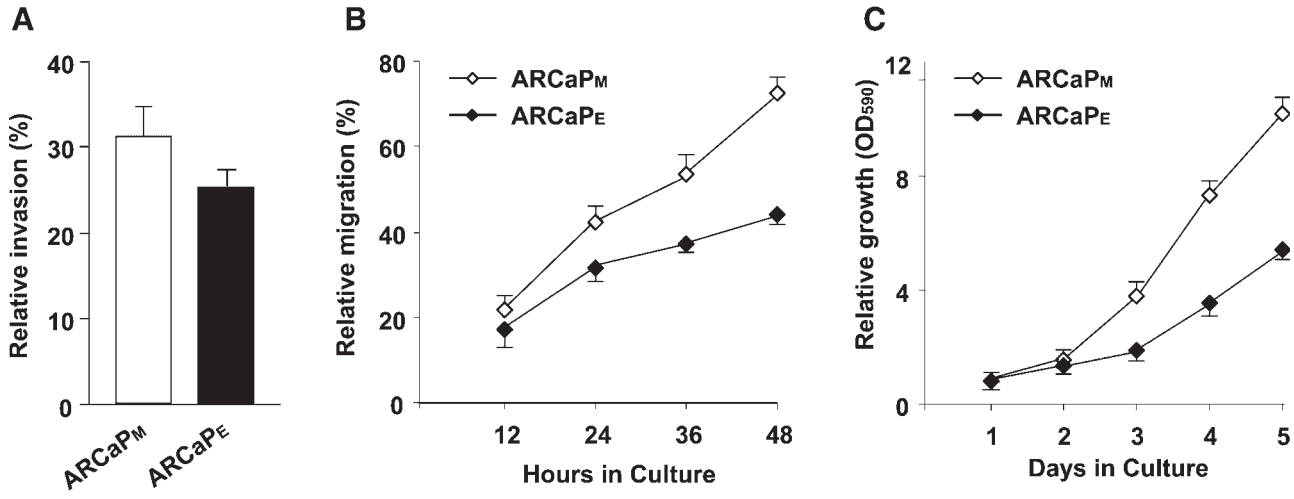

Fig. 2. $ARCaP_M$ cells exhibit higher invasion (**A**), migration (**B**), and growth rate (**C**) than $ARCaP_E$.

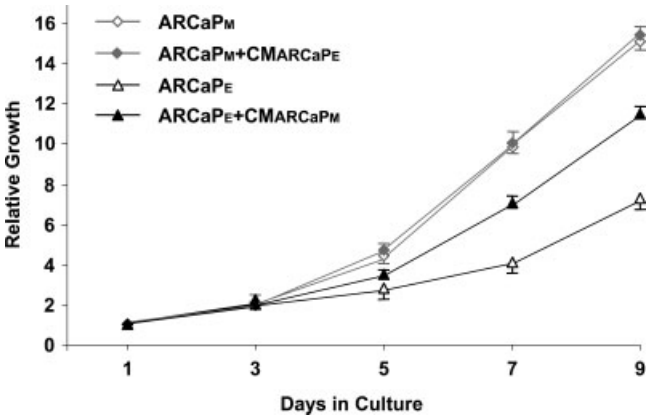

Fig. 3. Conditioned medium derived from fast-growing $ARCaP_M$ subclone stimulated the growth of slow-growing $ARCaP_E$ cells.

$ARCaP_M$ to several clinically used chemotherapeutic drugs and compared the results to invasive LNCaP lineage C4-2 cells treated with the same drugs. We found that $ARCaP_M$ and $ARCaP_E$ are more resistant to a DNA intercalating agent, doxorubicin (IC50s 5.5 and 3.4 uM for $ARCaP_M$ and $ARCaP_E$, respectively) than C4-2 cells (IC50, 2.7 uM). $ARCaP_M$ and $ARCaP_E$ are also more resistant to topoisomerase inhibitor II, etoposide (IC50s 5.8 and 8.1 uM, respectively) than C4-2 cells (IC50, 5.6 uM). The relative resistance of $ARCaP_M$ and $ARCaP_E$, compared to C4-2 cells, to the microtubule/tubulin assembly binding agent, paclitaxel, was also observed with IC50s at 39, 53, and 23.5 nM, respectively.

Comparison of the Tumorigenicity and Metastatic Potentials of $ARCaP_E$ and $ARCaP_M$ in Mice, and the Derivation of $ARCaP_M$-Like Cells From Bone and Adrenal Gland Harvested From Animals Inoculated With $ARCaP_E$ Cells

To confirm that differences in morphology, cell behavior, gene expression profiles, and sensitivity to chemotherapeutic drugs between ARCaP cell subclones in vitro reflect their tumorigenicity and metastatic potential in vivo, we conducted animal studies by inoculating two ARCaP cell subclones, $ARCaP_E$, and $ARCaP_M$, into the left ventricles of immune-compromised SCID mice. The animals were observed closely and bone and soft tissue metastases were confirmed by X-ray, physical palpation, and histomorphology. Figure 5 showed the histopathology (top panels) and vimentin expression (IHC, bottom panels) of primary tumors from $ARCaP_E$, $ARCaP_M$, and metastatic lesions of bone and adrenal gland in mice inoculated intracardiacally with ARCaP cells. Similar to our experience in the orthotopic injection of parental ARCaP cells [16], tumor cells induced mixed osteoblastic and osteolytic responses in mice upon intracardiac injection of ARCaP subclones. Some mice also exhibited apparent cachexia and paraplegia at the later stage of bone metastasis (data not included).

The EMT-associated elevated expression of vimentin was demonstrated in ARCaP bone and adrenal meatastatic tumors as comparing with the primary tumor (Fig. 5). We derived ARCaP cell subclones from bone and adrenal gland metastases and further tested

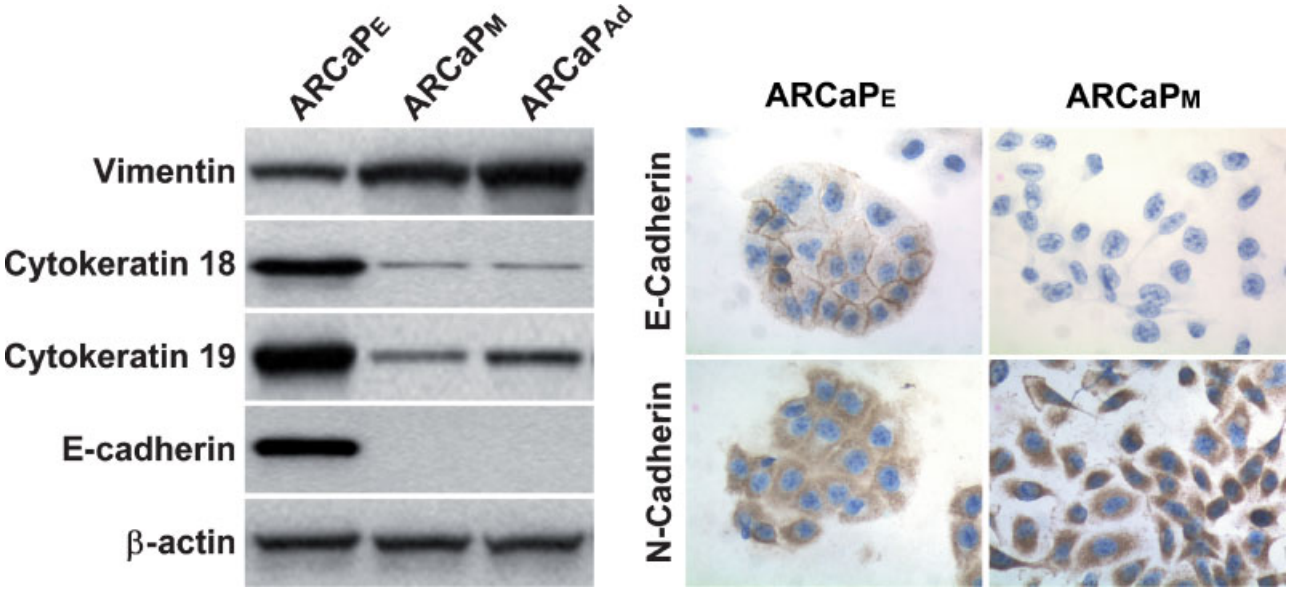

Fig. 4. Protein expression profile changes from $ARCaP_E$ to $ARCaP_M$ and $ARCaP_{Ad}$ are closely associated with epithelial to mesenchymal transition. Western blot (**left panel**), IHC (**right panel**).

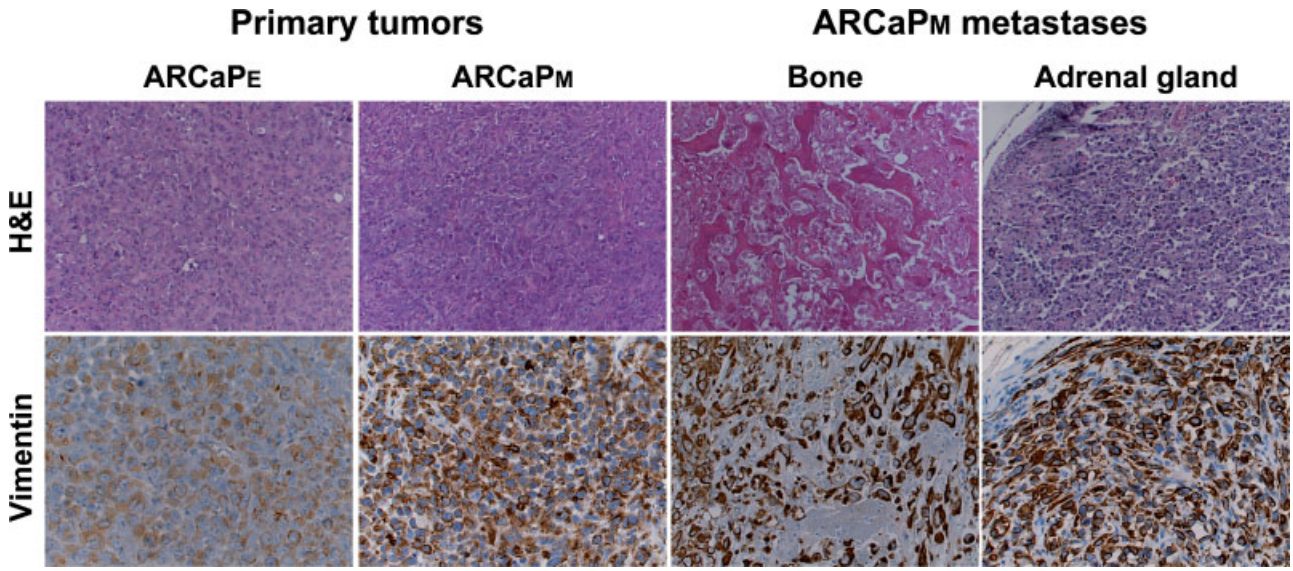

Fig. 5. Histomorphology (**top panel**) and vimentin expression (IHC, **bottom panel**) of primary tumors of $ARCaP_E$, $ARCaP_M$, metastatic bone, and adrenal gland induced by intracardiac injections of $ARCaP_M$ cells in athymic mice.

their metastatic potentials in mice. The incidence of bone metastasis ranged from 12.5% (1/8) for $ARCaP_E$ cells, with a latency of 71 days, to 100% (9/9) for $ARCaP_M$ cells, with a latency of 61 days (range 40–104 days). Interestingly, consistent with these observations, increased bone metastasis resulted from ARCaP cell interaction with mouse bone, through recycling of the injected $ARCaP_E$ or $ARCaP_M$ cells in the mouse hosts. Mice inoculated with $ARCaP_E$ or $ARCaP_M$ cells also developed increased adrenal gland metastasis, from 22% (4/18, latency 132 days, range 70–165 days) to 33% (3/9, latency 96 days, range 77 to 135 days). Remarkably, $ARCaP_{Ad}$ metastasized only to host adrenal gland. We observed that both $ARCaP_{Ad}$ and $ARCaP_M$-like cells derived from $ARCaP_E$ had altered morphology and gene expression profiles (Fig. 4) resembled mesenchymal cells, suggesting that the bone and adrenal gland microenvironments had promoted EMT by facilitating the trans-differentiation of $ARCaP_E$ cells toward $ARCaP_M$ with preferential metastasis to bone or adrenal gland. In addition to adrenal gland, a low frequency of host mice also developed lymph node, liver, and lung metastases (data not included).

DISCUSSION

We established an ARCaP human prostate cancer cell model to study the possible relationship between the host microenvironment, EMT, the critical transition of prostate cancer cells from epithelial to mesenchymal phenotype, [29–31], and the propensity of prostate cancer to metastasize to bone and soft tissue. We also correlated EMT with increased cell growth, migration, and invasion in vitro. EMT has been reported during embryonic development. The invasion front of the developing organ resembles that of the tumor, exhibiting increased cell motility, invasion, and migration as observed in breast and bladder cancers. In the ARCaP human prostate cancer progression model, EMT can be promoted by cellular interaction between an ARCaP human prostate cancer cell subclone, $ARCaP_E$, and host bone or adrenal gland. The derivative $ARCaP_M$ and $ARCaP_{Ad}$ cells have the propensity to metastasize to bone and adrenal gland, respectively. Through further cellular interaction with host adrenal gland, we derived a secondary generation of $ARCaP_{Ad}$ cells. We observed, remarkably, that second generation $ARCaP_{Ad}$ cells had their ability to metastasize restricted only to the host adrenal gland. Because of the similarities in cell morphology, gene expression profiles, and behavior of $ARCaP_M$ derived from $ARCaP_E$ through in vivo selection as a bone metastasis variant and the $ARCaP_M$ IA8 subclone originally isolated from the ARCaP cells, we suggest that IA8 derived from IF11 through EMT transdifferentiation and the interaction of $ARCaP_E$ with the host bone. Following cellular interaction between human prostate cancer $ARCaP_E$ cells and the mouse host, we observed changes in morphology, gene expression, and behavior in this cell clone to resemble a mesenchymal cell type, express mesenchymal genes, and show increased invasion and migration in vitro and metastasis to bone and adrenal gland in live mice (Fig. 2–5). The changes in gene expression profile, such as increased expression of vimentin and N-cadherin and decreased expression of E-cadherin and cytokeratin18 and 19, are consistent

with the morphologic switch of ARCaP cells by EMT, with increased metastatic potential, as reported in several other tumor types [32–35]. We suggest that the host microenvironment plays an important role in facilitating EMT and subsequent prostate cancer metastasis to the skeleton and soft tissues [3]. We observed that despite the clonal origin of ARCaP cells, they present as distinct morphologic and molecular variants with diverse ability to metastasize to bone and adrenal gland. Our results suggest that soluble stimulatory factor(s) secreted by prostate cancer cells may be responsible for the maintenance of tumor cell heterogeneity in ARCaP cells when cultured in vitro (Fig. 3). These observations are consistent with the published literature, where soluble factors such as TGFβ and/or EGF can confer EMT in cultured cells, resulting in altered cell growth and behaviors such as cell motility, invasion, and metastasis in vitro [29,31,33,35].

The fact that host interaction enhances EMT and promotes ARCaP cells to migrate, invade, and metastasize in this model suggests that clinical bone and adrenal gland metastases of prostate cancer cells may be acquired and facilitated by cellular interaction with host microenvironment. Based on the results of this and our previous studies [3,15,16,26], it is likely that resident fibroblasts in the prostate, bone, or adrenal gland or cells recruited from hosts, such as inflammatory and marrow stem cells [36–38], can instigate prostate cancer cells to gain increased malignant potential through the local production of soluble factors, reactive oxygen species and/or extracellular matrices that prompt the tumor cells for enhanced growth and metastasis [30,35,37,38]. Using marginally tumorigenic LNCaP cells as model, we showed previously that co-inoculating LNCaP cells with either non-tumorigenic human prostate stromal fibroblast or a human osteosarcoma cell line [25,39] formed large chimeric tumors. By cloning LNCaP cells from the chimeric tumors, we established lineage-derived LNCaP sublines C4-2 and C4-2B cells which, like other variants [25,39,40], exhibited increased lymph node and bone metastasis. Similar results, that is, an increased propensity for local tumor formation and distant metastases, were obtained with ARCaP cells as described in the present communication and other human prostate cancer cell lines, whereby a human prostate cancer cell line when injected alone, without the presence of stromal fibroblasts, but with recruited host stromal cells, can promote prostate cancer progression [41–43]. We posit that ARCaP interaction with bone or adrenal gland promotes irreversible EMT with subsequent increased invasive and migratory potential and the ability to metastasize to bone and soft tissues.

The demonstration that ARCaP cells undergo EMT in bone or adrenal gland and gain metastatic potential for various sites has several important clinical implications for controlling cancer growth and metastasis. First, the host microenvironment includes soluble and insoluble factors associated with or secreted by osteoblasts, osteoclasts, marrow stromal, or stem cells that could play key roles promoting EMT, an important molecular transition by which cancer cells gain increased metastatic potential in response to the changing tumor microenvironment. These interactions could result in the promotion of cancer cell metastasis to soft tissues such as the adrenal gland, a documented site for human prostate cancer metastasis [44]. Second, if EMT acquired by prostate cancer cells following cellular interaction with host bone or adrenal gland occurs in patients, this could be a potential target for prevention and treatment strategies. Third, since the host microenvironment was shown to promote EMT and prostate cancer progression, host-stroma-directed targeting of prostate cancer such as by the use of atrasentan [45], bisphosphonates [46], growth factor receptor antagonists [47], antiangiogenics [48], and radiopharmaceuticals [49], should be further explored to improve the treatment of cancer metastases.

CONCLUSIONS

We demonstrated that the host microenvironment is a critical site for the transition of human prostate cancer cells from epithelial to mesenchymal morphology, resulting in increased metastatic potential for bone and adrenal gland. Clonal prostate cancer cells could have different histomorphologies, gene expression profiles, sensitivity toward cancer therapeutic drugs, and variable behaviors in culture and in the host. We found that clonal interaction, possibly mediated by soluble factors secreted by prostate cancer cells, is responsible for maintaining tumor cell heterogeneity. Our study documented that EMT can be facilitated through cellular interaction between human prostate cancer cells and mouse skeleton or adrenal gland and that EMT could be exploited as a potential target for the prevention and treatment of human prostate cancer metastases.

ACKNOWLEDGMENTS

We thank Yuanyuan Cui, Shari Kelly and Carol Phillips for technical supports and Gary Mawyer for editing. The study was supported by R01 CA082739 to HYEZ; PC 040267 to VOM; and PO1 CA098912 and CA 108468 and PC040260 to LWKC.

REFERENCES

1. Bavik C, Coleman I, Dean JP, Knudsen B, Plymate S, Nelson PS. The gene expression program of prostate fibroblast senescence modulates neoplastic epithelial cell proliferation through paracrine mechanisms. Cancer Res 2006;66(2):794–802.
2. Barrett JM, Mangold KA, Jilling T, Kaul KL. Bi-directional interactions of prostate cancer cells and bone marrow endothelial cells in three-dimensional culture. Prostate 2005;64(1):75–82.
3. Chung LW, Baseman A, Assikis V, Zhau HE. Molecular insights into prostate cancer progression: The missing link of tumor microenvironment. J Urol 2005;173(1):10–20.
4. Bova GS, Parmigiani G, Epstein JI, Wheeler T, Mucci NR, Rubin MA. Web-based tissue microarray image data analysis: Initial validation testing through prostate cancer Gleason grading. Hum Pathol 2001;32(4):417–427.
5. DeMarzo AM, Nelson WG, Isaacs WB, Epstein JI. Pathological and molecular aspects of prostate cancer. Lancet 2003;361(9361): 955–964.
6. Carter HB, Piantadosi S, Isaacs JT. Clinical evidence for and implications of the multistep development of prostate cancer. J Urol 1990;143(4):742–746.
7. De S, Chen J, Narizhneva NV, Heston W, Brainard J, Sage EH, Byzova TV. Molecular pathway for cancer metastasis to bone. J Biol Chem 2003;278(40):39044–39050.
8. Kasper S, Sheppard PC, Yan Y, Pettigrew N, Borowsky AD, Prins GS, Dodd JG, Duckworth ML, Matusik RJ. Development, progression, and androgen-dependence of prostate tumors in probasin-large T antigen transgenic mice: A model for prostate cancer. Lab Invest 1998;78(6):i–xv.
9. Greenberg NM. Androgens and growth factors in prostate cancer: A transgenic perspective. Prostate Cancer Prostatic Dis 2000;3(4):224–228.
10. Garabedian EM, Humphrey PA, Gordon JI. A transgenic mouse model of metastatic prostate cancer originating from neuroendocrine cells. Proc Natl Acad Sci USA 1998;95(26):15382–15387.
11. Yonou H, Yokose T, Kamijo T, Kanomata N, Hasebe T, Nagai K, Hatano T, Ogawa Y, Ochiai A. Establishment of a novel species- and tissue-specific metastasis model of human prostate cancer in humanized non-obese diabetic/severe combined immunodeficient mice engrafted with human adult lung and bone. Cancer Res 2001;61(5):2177–2182.
12. Wang Y, Xue H, Cutz JC, Bayani J, Mawji NR, Chen WG, Goetz LJ, Hayward SW, Sadar MD, Gilks CB, Gout PW, Squire JA, Cunha GR, Wang YZ. An orthotopic metastatic prostate cancer model in SCID mice via grafting of a transplantable human prostate tumor line. Lab Invest 2005;85(11):1392–1404.
13. Nemeth JA, Harb JF, Barroso U Jr, He Z, Grignon DJ, Cher ML. Severe combined immunodeficient-hu model of human prostate cancer metastasis to human bone. Cancer Res 1999;59(8):1987–1993.
14. Navone NM, Olive M, Ozen M, Davis R, Troncoso P, Tu SM, Johnston D, Pollack A, Pathak S, von Eschenbach AC, Logothetis CJ. Establishment of two human prostate cancer cell lines derived from a single bone metastasis. Clin Cancer Res 1997;3(12 Pt 1):2493–2500.
15. Wu TT, Sikes RA, Cui Q, Thalmann GN, Kao C, Murphy CF, Yang H, Zhau HE, Balian G, Chung LW. Establishing human prostate cancer cell xenografts in bone: Induction of osteoblastic reaction by prostate-specific antigen-producing tumors in athymic and SCID/bg mice using LNCaP and lineage-derived metastatic sublines. Int J Cancer 1998;77(6):887–894.
16. Zhau HY, Chang SM, Chen BQ, Wang Y, Zhang H, Kao C, Sang QA, Pathak SJ, Chung LW. Androgen-repressed phenotype in human prostate cancer. Proc Natl Acad Sci USA 1996;93(26): 15152–15157.
17. Wainstein MA, He F, Robinson D, Kung HJ, Schwartz S, Giaconia JM, Edgehouse NL, Pretlow TP, Bodner DR, Kursh ED. CWR22: Androgen-dependent xenograft model derived from a primary human prostatic carcinoma. Cancer Res 1994;54(23): 6049–6052.
18. Corey E, Quinn JE, Buhler KR, Nelson PS, Macoska JA, True LD, Vessella RL. LuCaP 35: A new model of prostate cancer progression to androgen independence. Prostate 2003;55(4): 239–246.
19. Carter BS, Beaty TH, Steinberg GD, Childs B, Walsh PC. Mendelian inheritance of familial prostate cancer. Proc Natl Acad Sci USA 1992;89(8):3367–3371.
20. Visakorpi T, Kallioniemi AH, Syvanen AC, Hyytinen ER, Karhu R, Tammela T, Isola JJ, Kallioniemi OP. Genetic changes in primary and recurrent prostate cancer by comparative genomic hybridization. Cancer Res 1995;55(2):342–347.
21. Gronberg H, Damber L, Damber JE. Studies of genetic factors in prostate cancer in a twin population. J Urol 1994;152(5 Pt 1): 1484–1487; discussion 1487–1489.
22. Sikes RA, Nicholson BE, Koeneman KS, Edlund NM, Bissonette EA, Bradley MJ, Thalmann GN, Cecchini MG, Pienta KJ, Chung LW. Cellular interactions in the tropism of prostate cancer to bone. Int J Cancer 2004;110(4):497–503.
23. Huang H, Muddiman DC, Tindall DJ. Androgens negatively regulate forkhead transcription factor FKHR (FOXO1) through a proteolytic mechanism in prostate cancer cells. J Biol Chem 2004; 279(14):13866–13877.
24. Wu YM, Robinson DR, Kung HJ. Signal pathways in up-regulation of chemokines by tyrosine kinase MER/NYK in prostate cancer cells. Cancer Res 2004;64(20):7311–7320.
25. Gleave M, Hsieh JT, Gao CA, von Eschenbach AC, Chung LW. Acceleration of human prostate cancer growth in vivo by factors produced by prostate and bone fibroblasts. Cancer Res 1991; 51(14):3753–3761.
26. Thalmann GN, Sikes RA, Wu TT, Degeorges A, Chang SM, Ozen M, Pathak S, Chung LW. LNCaP progression model of human prostate cancer: Androgen-independence and osseous metastasis. Prostate 2000;44(2):91–103 Jul 101;144(102).
27. Hoosein NM, Logothetis CJ, Chung LW. Differential effects of peptide hormones bombesin, vasoactive intestinal polypeptide and somatostatin analog RC-160 on the invasive capacity of human prostatic carcinoma cells. J Urol 1993;149(5):1209–1213.
28. Kariya Y, Miyazaki K. The basement membrane protein laminin-5 acts as a soluble cell motility factor. Exp Cell Res 2004;297(2): 508–520.
29. Huber MA, Kraut N, Beug H. Molecular requirements for epithelial-mesenchymal transition during tumor progression. Curr Opin Cell Biol 2005;17(5):548–558.
30. Thiery JP. Epithelial-mesenchymal transitions in development and pathologies. Curr Opin Cell Biol 2003;15(6):740–746.
31. Larue L, Bellacosa A. Epithelial-mesenchymal transition in development and cancer: Role of phosphatidylinositol 3′ kinase/AKT pathways. Oncogene 2005;24(50):7443–7454.
32. Cattan N, Rochet N, Mazeau C, Zanghellini E, Mari B, Chauzy C, Stora de Novion H, Amiel J, Lagrange JL, Rossi B, Gioanni J. Establishment of two new human bladder carcinoma cell lines, CAL 29 and CAL 185. Comparative study of cell scattering and

epithelial to mesenchyme transition induced by growth factors. Br J Cancer 2001;85(9):1412–1417.

33. Nawshad A, Lagamba D, Polad A, Hay ED. Transforming growth factor-beta signaling during epithelial-mesenchymal transformation: Implications for embryogenesis and tumor metastasis. Cells Tissues Organs 2005;179(1-2):11–23.
34. Han G, Lu SL, Li AG, He W, Corless CL, Kulesz-Martin M, Wang XJ. Distinct mechanisms of TGF-beta1-mediated epithelial-to-mesenchymal transition and metastasis during skin carcinogenesis. J Clin Invest 2005;115(7):1714–1723.
35. Kang Y, Massague J. Epithelial-mesenchymal transitions: Twist in development and metastasis. Cell 2004;118(3):277–279.
36. Aggarwal BB. Nuclear factor-kappaB: The enemy within. Cancer Cell 2004;6(3):203–208.
37. Kaplan RN, Riba RD, Zacharoulis S, Bramley AH, Vincent L, Costa C, MacDonald DD, Jin DK, Shido K, Kerns SA, Zhu Z, Hicklin D, Wu Y, Port JL, Altorki N, Port ER, Ruggero D, Shmelkov SV, Jensen KK, Rafii S, Lyden D. VEGFR1-positive haematopoietic bone marrow progenitors initiate the pre-metastatic niche. Nature 2005;438(7069):820–827.
38. Reya T, Clevers H. Wnt signalling in stem cells and cancer. Nature 2005;434(7035):843–850.
39. Thalmann GN, Anezinis PE, Chang SM, Zhau HE, Kim EE, Hopwood VL, Pathak S, von Eschenbach AC, Chung LW. Androgen-independent cancer progression and bone metastasis in the LNCaP model of human prostate cancer. Cancer Res 1994; 54(10):2577–2581.
40. Rhee HW, Zhau HE, Pathak S, Multani AS, Pennanen S, Visakorpi T, Chung LW. Permanent phenotypic and genotypic changes of prostate cancer cells cultured in a three-dimensional rotating-wall vessel. In Vitro Cell Dev Biol Anim 2001;37(3):127–140.
41. Sramkoski RM, Pretlow TG 2nd, Giaconia JM, Pretlow TP, Schwartz S, Sy MS, Marengo SR, Rhim JS, Zhang D, Jacobberger JW. A new human prostate carcinoma cell line, 22Rv1. In Vitro Cell Dev Biol Anim 1999;35(7):403–409.
42. Pettaway CA, Pathak S, Greene G, Ramirez E, Wilson MR, Killion JJ, Fidler IJ. Selection of highly metastatic variants of different human prostatic carcinomas using orthotopic implantation in nude mice. Clin Cancer Res 1996;2(9):1627–1636.
43. Klein KA, Reiter RE, Redula J, Moradi H, Zhu XL, Brothman AR, Lamb DJ, Marcelli M, Belldegrun A, Witte ON, Sawyers CL. Progression of metastatic human prostate cancer to androgen independence in immunodeficient SCID mice. Nat Med 1997; 3(4):402–408.
44. Bates AW, Baithun SI. Secondary solid neoplasms of the prostate: A clinico-pathological series of 51 cases. Virchows Arch 2002;440(4):392–396.
45. Nelson JB, Nabulsi AA, Vogelzang NJ, Breul J, Zonnenberg BA, Daliani DD, Schulman CC, Carducci MA. Suppression of prostate cancer induced bone remodeling by the endothelin receptor A antagonist atrasentan. J Urol 2003;169(3):1143–1149.
46. Smith MR. Zoledronic acid to prevent skeletal complications in cancer: Corroborating the evidence. Cancer Treat Rev 2005; 31(Suppl 3):19–25.
47. Wu JD, Odman A, Higgins LM, Haugk K, Vessella R, Ludwig DL, Plymate SR. In vivo effects of the human type I insulin-like growth factor receptor antibody A12 on androgen-dependent and androgen-independent xenograft human prostate tumors. Clin Cancer Res 2005;11(8):3065–3074.
48. Longoria RL, Cox MC, Figg WD. Antiangiogenesis: A possible treatment option for prostate cancer? Clin Genitourin Cancer 2005;4(3):197–202.
49. Tu SM, Millikan RE, Mengistu B, Delpassand ES, Amato RJ, Pagliaro LC, Daliani D, Papandreou CN, Smith TL, Kim J, Podoloff DA, Logothetis CJ. Bone-targeted therapy for advanced androgen-independent carcinoma of the prostate: A randomised phase II trial. Lancet 2001;357(9253):336–341.

An ultrasensitive imaging technique utilizing near-infrared fluorescent quantum dots for the detection of human prostate cancer bone metastasis in a mouse xenograft model

Chunmeng Shi, Zhihui Xie, Chia-Ling Hsieh, *Shuming Nie, Haiyen E. Zhau, and Leland W.K. Chung

Department of Urology, and *Department of Biomedical Engineering, Winship Cancer Institute, Emory University School of Medicine, Atlanta, GA 30322, USA

The application of near-infrared (NIR) fluorescent probes is a promising approach for *in vivo* biomedical imaging due to low tissue scattering and absorption, which yields greater tissue penetration and a favorable optical signal in this region of the electromagnetic spectrum. Conventional NIR organic fluorophores suffer from low quantum yield, broad emission spectra and photo-bleaching. Quantum dots (QDs) offer an excellent alternative to organic fluorophores to overcome these limitations. Here, we show the *in vivo* imaging of human prostate cancer cells growing as tumors in mouse skeleton by bioconjugated NIR QD probes. QDs with the emission peak of 800 nm were conjugated to a monoclonal antibody, J591 (Millennium), for human prostate-specific membrane antigen (PSMA). QD images in culture and in implanted tumors in mice were acquired using the IVIS imaging system. A sequence of images taken with narrow band emission filters was used to subtract the tissue autofluorescence background. Autofluorescence was also significantly minimized and avoided with an alpha-free-diet. The PSMA antibody-conjugated QD probes showed strong and specific binding of the hormone-refractory human prostate cancer cell line, C4-2B, which is known to express PSMA on the cell surface and is able to metastasize to the bone. QDs did not affect cancer cell viability and growth *in vitro*. We determined the sensitivity of this fluorescence imaging method by first inoculating C4-2B cells in mice either subcutaneously or intra-tibially and then tracking the location of C4-2B cells and tumors by systemic injection of QD-tagged PSMA antibody. We have shown a linear correlation between the fluorescent signal and the cell number following either subcutaneous or intratibial implantation of QD-tagged

C4-2B cells. With systemic injection of PSMA-conjugated QD probes, we found a minimal detection limit of cancer cells in the mouse tibia of about 500,000 cells (~0.5 mg of tumor), which is at least 1,000-fold more sensitive than the current detection methods used clinically. In comparative studies, both fluorescent signals from 655 nm QDs and GFP stably transfected C4-2B cells could not be detected due to interference by the background autofluorescence. A time-course study with systemic injection of uncoated QDs by tail vein showed accumulation of QDs in the liver and lymph nodes within 30 minutes of injection; the fluorescence remained there over 15 days. Surface modification of QDs with PEG resulted in substantially longer circulation time without significant uptake by the liver and lymph nodes up to 2 hours after tail vein injection. Our results established the use of bioconjugated NIR QD probes for the molecular imaging of human prostate cancer in deep tissues, and offer a significantly improved method of detecting human prostate cancer micrometastases in bone.

Appendix 3

Cell signaling mediating by β2-microglobulin and protein kinase A promotes growth and epithelial to mesenchymal transition in human renal cancers

Takeo Nomura, Wen-Chin Haung, Yun Xing, Andrew N. Young, Fray F. Marshall, Shuming Nie, Haiyen E. Zhau, and Leland W.K. Chung, Atlanta, Georgia

Introduction and Objective: β2-microglobulin (β2M), a unique soluble factor secreted by renal cancer and host inflammatory cells, increases anchorage-dependent and independent growth of renal cancer cells in culture and promotes epithelial to mesenchymal transition (EMT), associated with increased cell motility, migration and invasion in kidney morphogenesis. β2M-mediated cell signaling promoted growth, survival and osteomimesis of renal cancer cells and may determine their metastatic potential.

Methods: We overexpressed β2M in human SN12C renal cancer cells using an expression plasmid cDNA encoding β2M (control cells were stably tranfected with neo expression construct) and correlated β2M expression levels with: 1) in vitro growth, both on plastic dishes and as Matrigel colonies; 2) cell migration and invasion in a Boyden chamber; and 3) expression of EMT markers, E-cadherin, N-cadherin, vimentin, receptor activator of NF-kB ligand (RANKL) assessed by RT-PCR for mRNA and western blot and a multiplexing quantum dot-based immunohistochemical (QD-IHC) assay for protein. Clinical significance of β2M was assessed by evaluating its expression by IHC in 12 human renal cancer specimens (2, 5 and 5 G1, G2 and G3 clear cell carcinoma specimens).

Results: In SN12C cells stably expressing β2M (2.5 and 6.1 fold more β2M than in neo transfected clones by ELISA), steady-state levels of β2M expression correlated positively with cell proliferation both on plastic and in Matrigel, cell motility, and invasion *in vitro*. SN12C cells and neo transfected clones had a smooth spherical appearance. β2M overexpressing cells had a stellate morphology in Matrigel. β2M overexpression promoted EMT, with significantly decreased E-cadherin and increased N-cadherin, vimentin, and RANKL at both protein, assayed by QD-IHC and western, and mRNA levels. β2M was detected by IHC in all renal cancer tissues but was sparse only found in the luminal border of benign kidney tubules. β2M was membrane-bound in all cancer cases; two cases expressed focally in cell cytoplasm. β2M levels in cancer cells and normal kidney tubules were significantly different, but not clearly associated with tumor grade.

Conclusions: β2M is a novel mitogen supporting growth, EMT, and migration and invasion by human renal cancer cells. β2M, expressed in the cell membrane and cytoplasm of cancer but not normal kidney cells, could be a new diagnostic and prognostic marker for human renal cancers.

Figure 1

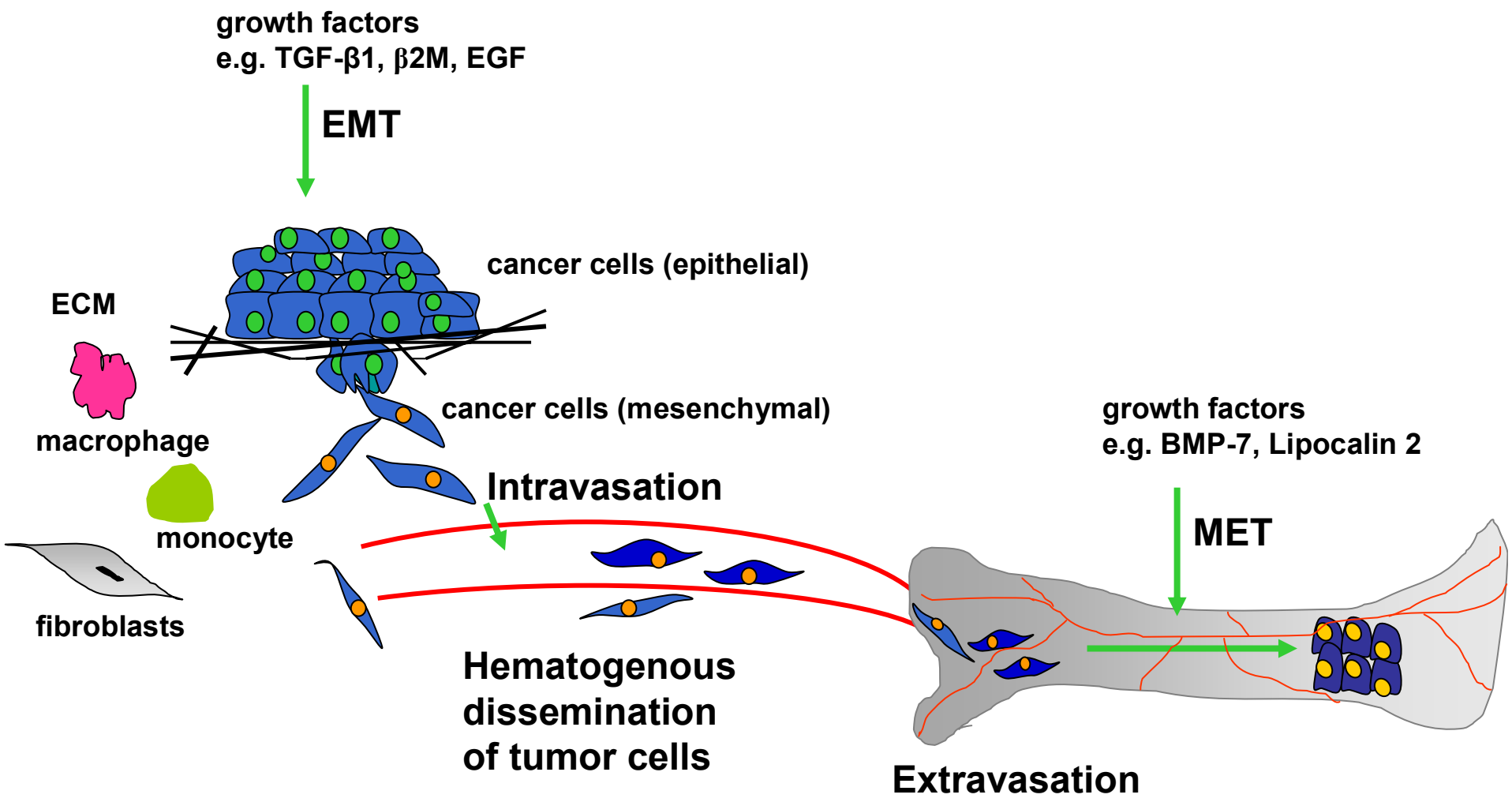
growth factors
e.g. TGF-β1, β2M, EGF
EMT
cancer cells (epithelial)
ECM
macrophage
cancer cells (mesenchymal)
Intravasation
monocyte
fibroblasts
growth factors
e.g. BMP-7, Lipocalin 2
MET
Hematogenous
dissemination
of tumor cells
Extravasation

Figure 2

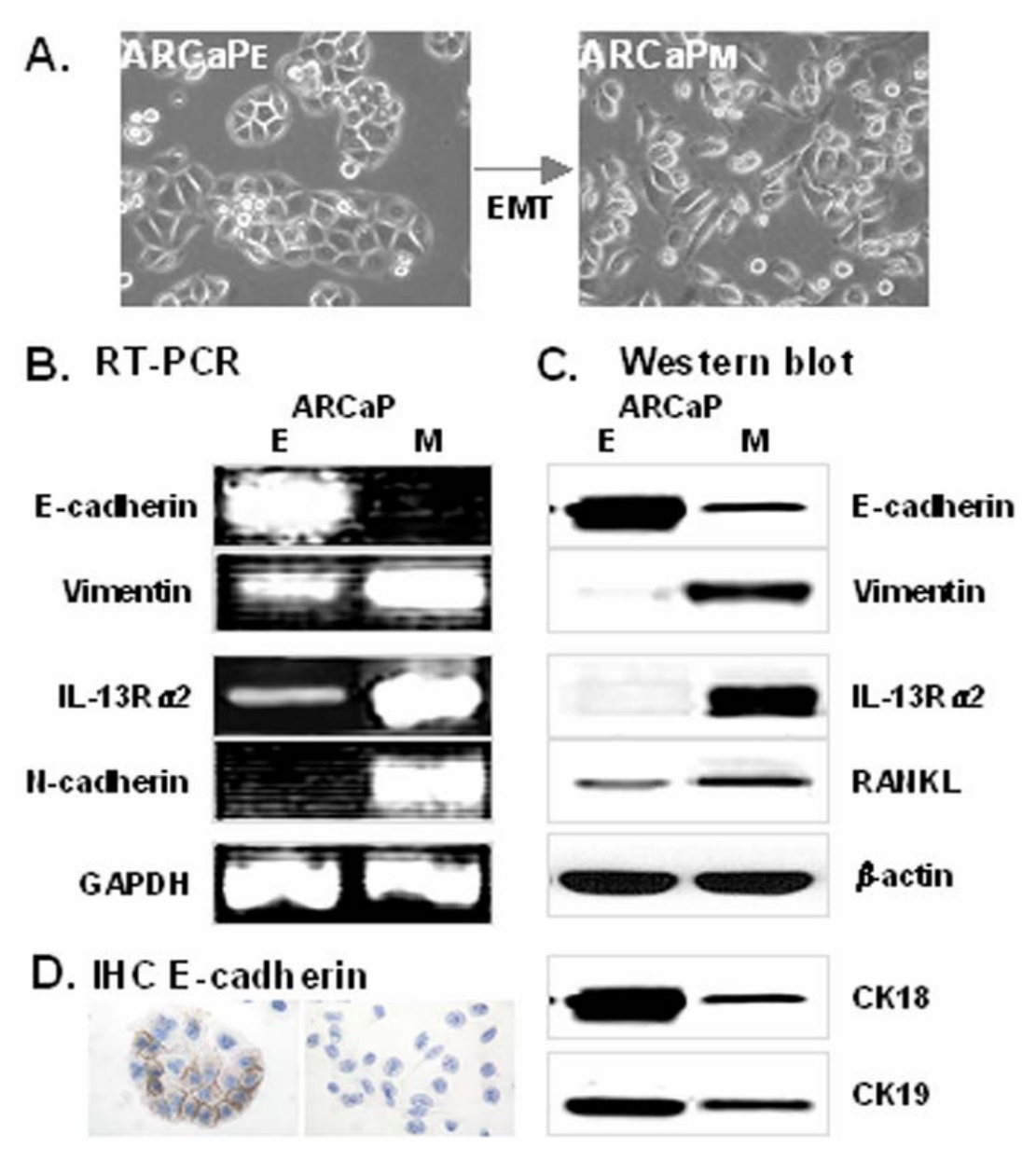
A.
ARCaPE
EMT
ARCaPM
B. RT-PCR
ARCaP
E
M
E-cadherin
Vimentin
IL-13Rα2
N-cadherin
GAPDH
C. Western blot
ARCaP
E
M
E-cadherin
Vimentin
IL-13Rα2
RANKL
β-actin
CK18
CK19
D. IHC E-cadherin

Figure 3

QD multi-staining of ARCaP$_E$

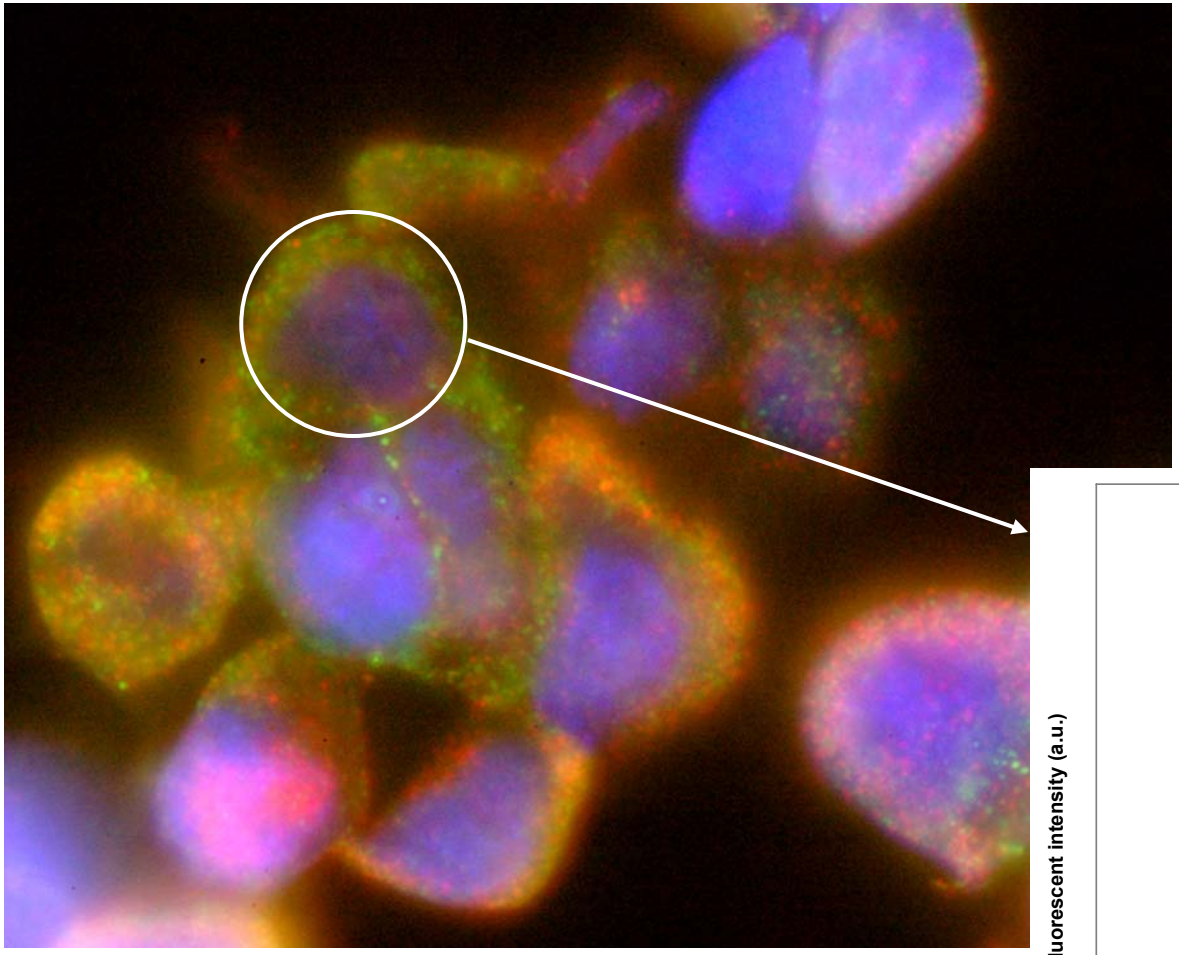

E-cadherin (QD565, green)

N-cadherin (QD605, red)

Ki-67 (QD655, red)

Nuclei (DAPI, blue)

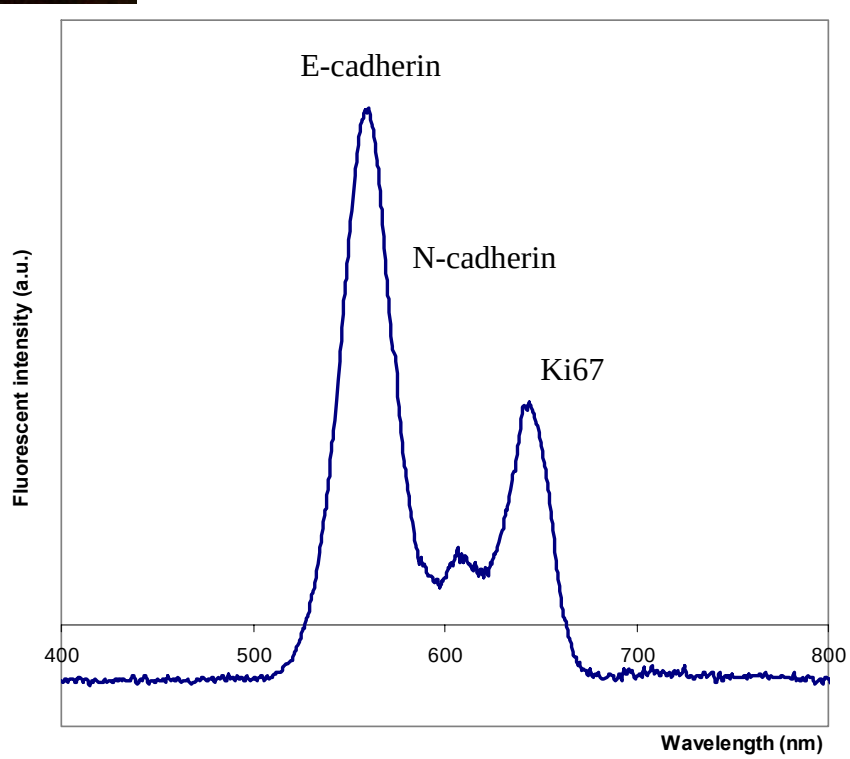

Yun Xing & Takeo Nomura, 2005

Figure 4

QD multi-staining of $ARCaP_M$

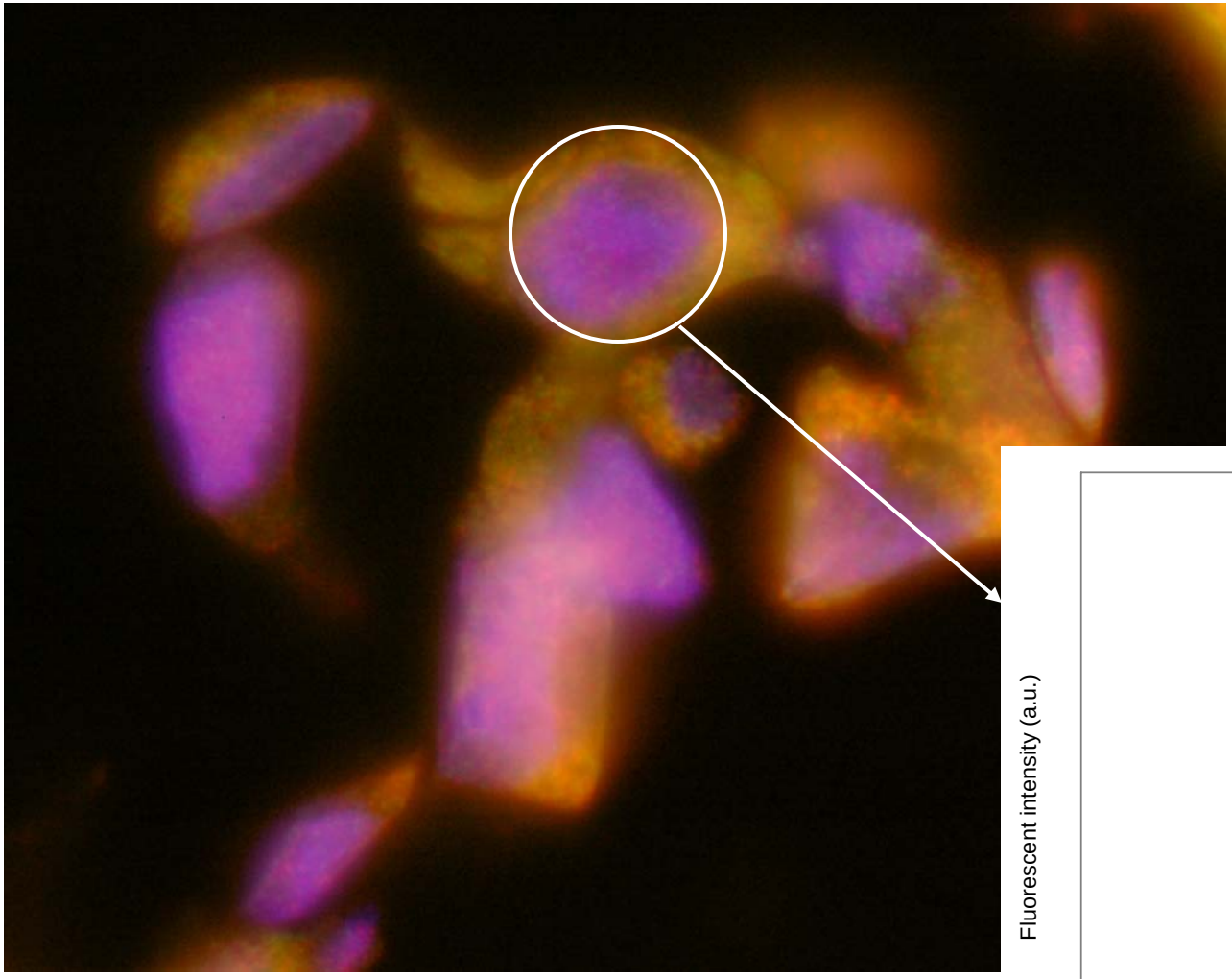

E-cadherin (QD565, green)

N-cadherin (QD605, red)

Ki-67 (QD655, red)

Nuclei (DAPI, blue)

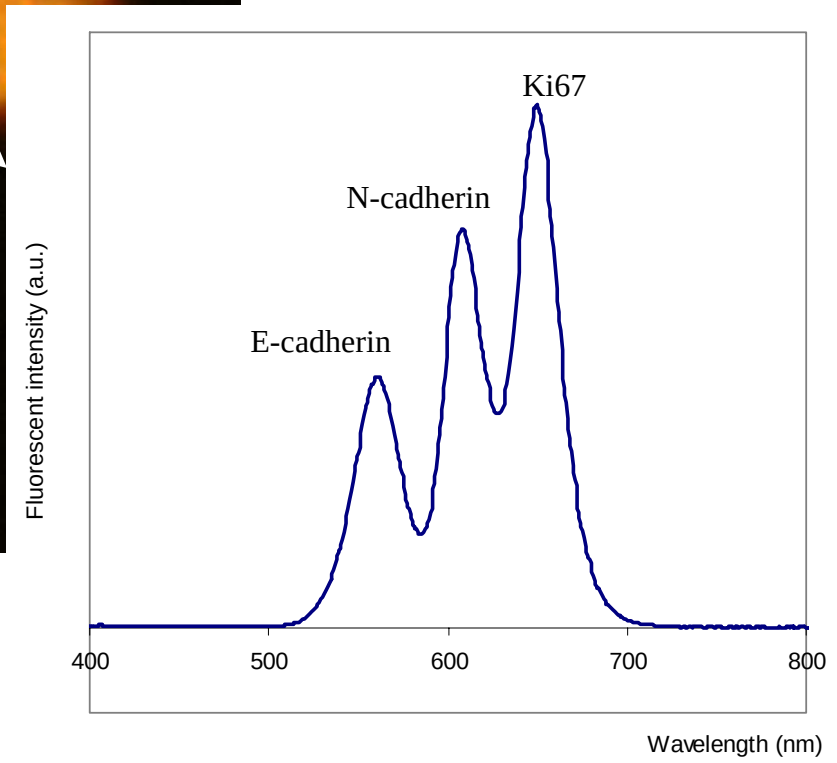

Yun Xing & Takeo Nomura, 2005

Figure 5

IL-13Ra2 (655): $ARCaP_E$ (left) vs. $ARCaP_M$ (right) tumor tissues